Stability of evaporating water when heated through the vapor and the liquid phases

Kausik S. Das, Brendan D. MacDonald, and C. A. Ward*
Thermodynamics and Kinetics Laboratory, Department of Mechanical and Industrial Engineering, University of Toronto, Toronto, Canada M5S 3G8

(Received 15 August 2009; revised manuscript received 11 January 2010; published 23 March 2010)

The stability of a water layer of uniform thickness held in a two-dimensional container of finite or semi-infinite extent is examined using linear stability theory. The liquid-vapor interface can be heated both through the liquid and through the vapor, as previously experimentally reported. The need to introduce a heat transfer coefficient is eliminated by introducing statistical rate theory (SRT) to predict the evaporation flux. There are no fitting or undefined parameters in the expression for the evaporation flux. The energy transport is parametrized in terms of the evaporation number, E_{ev}, that for a given experimental circumstance can be predicted. The critical Marangoni number for the finite, Ma_{cf}, and for the semi-infinite system, $\mathrm{Ma}_{c\infty}$, can be quantitatively predicted. Experiments in which water evaporated from a stainless-steel funnel and from a polymethyl methacrylate (PMMA) funnel into its vapor have been previously reported. Marangoni convection was observed in the experiments that used the stainless-steel funnel but not with the PMMA funnel even though the Marangoni number for the PMMA funnel was more than 27 000. The SRT-based stability theory indicates that the critical value of the Marangoni number for the experiments with the PMMA funnel was greater than the experimental value of the Marangoni number in each case; thus, no Marangoni convection was predicted to result from an instability. The observed convection with the stainless-steel funnel resulted from a temperature gradient imposed along the interface.

DOI: 10.1103/PhysRevE.81.036318 PACS number(s): 47.20.Dr, 47.55.dm

I. INTRODUCTION

The conditions at the liquid-vapor interface during phase-change processes have proven to be surprisingly complex. Earlier experimental studies have indicated that on the center line of an axisymmetric liquid phase evaporating into its vapor while maintained at the circular mouth of a stainless-steel funnel, there are interfacial-temperature discontinuities in which the interfacial-vapor temperature is greater than that of the liquid and that the magnitude of the discontinuity depends on the evaporation flux [1–4]. Although these measurements were made with microthermocouples, the measurements have been used with statistical rate theory (SRT) [5] to predict the latent heat and constant pressure specific heat of water as functions of temperature that are in agreement with independently measured values of these properties [6]. We emphasize that the measured interfacial temperatures were used in the analysis, as opposed to temperatures measured at the funnel throat.

In contrast, Bond and Struchtrup used temperatures measured at the funnel throat as part of the inputs to their analysis to calculate the interfacial temperatures. They concluded that the energy flux is the dominant factor in determining the interfacial-temperature discontinuities and noted that the parameters in their analysis could be chosen to give good agreement with the experiments of Refs. [1,3] but that the classical-kinetic-theory-based Hertz-Knudsen and Schrage laws could not. The validity of the Hertz-Knudsen relation was also questioned by Hołyst and Litniewski [7] who used molecular dynamics to examine the evaporation into a vacuum from a liquid film. They also examined the evaporation of an enclosed nanosized droplet and concluded that the temperature discontinuity depended, in part, on how the vapor interacted with the enclosing walls [8]. It remains an open question of how the evaporation and condensation coefficients of the Hertz-Knudsen relation may be determined other than empirically [9,10].

However, neither the study by Bond and Struchtrup nor those of Hołyst and Litniewski included surface-tension-driven (or Marangoni or thermocapillary) convection in their analysis. Since in the experiments of references [1–3] the interfacial temperature was measured only on the funnel center line, from those measurements alone, it could not be established whether Marangoni convection existed. Even if buoyancy-driven convection was eliminated in these experiments, Marangoni convection could have contributed significantly to the energy transport in the bulk liquid [11–15].

In subsequent water evaporation experiments conducted with the same stainless-steel funnel, the interfacial temperatures were measured along the interface. In each experiment, the interfacial-temperature discontinuity persisted at positions along the interface, but as the interfacial evaporation flux was increased, a transition from quiescent water evaporation to evaporation with Marangoni convection occurred [16], but the mechanism by which the Marangoni convection was initiated was unclear (see below). Nonetheless, it was shown that an extraordinary amount of energy was transported by the Marangoni convection. The energy transport was defined in terms of the surface-thermal capacity, c_σ, and for one value of this surface property, the-conservation-of-energy principle was satisfied for each of nine water evaporation experiments conducted over a range of conditions [17]. The value of c_σ was confirmed in a second set of experiments in which the liquid-vapor interface was converted from spherical to cylindrical and the area increased by a factor of 4 [18]. It was hypothesized that the large value of

*charles.ward@utoronto.ca

c_σ resulted from the polar interactions of the water molecules. This hypothesis was supported by a third set of evaporation experiments that used D_2O as the test fluid. These experiments indicated the value of c_σ was similar to that of H_2O [19].

Since Marangoni convection is indicated to transport an extraordinary amount of thermal energy during water evaporation [20], it is important to determine under what conditions Marangoni convection is initiated in volatile liquids because it potentially offers a means of enhancing the efficiency of evaporation and thus has a number of important applications.

II. INITIATION OF MARANGONI CONVECTION DURING LIQUID EVAPORATION

In a recent paper, experiments were discussed in which water evaporated into its vapor while maintained at the circular mouth of a *PMMA funnel* with the funnel throat maintained at a constant temperature of ~3.5 °C [21]. No Marangoni convection was observed, even though the experimental Marangoni number was more than 12 times greater than the value of the Marangoni number predicted to be critical by the Pearson-Nield model [22,23]. Thus, on the basis of the Pearson-Nield model, Marangoni convection was expected, but no evidence of its presence was found.

In contrast, when H_2O and D_2O each evaporated into their respective vapors while maintained at the circular mouth of a *stainless-steel funnel* with the funnel throat also maintained at ~3.5 °C, Marangoni convection was clearly present [16,17,19], but the mechanism by which the convection was initiated was not clear. The value of the critical Marangoni number, Ma_{cr}, was in reasonable agreement with that predicted by the Pearson-Nield model (81 compared with ~147), but the possibility of thermal conduction from the funnel throat through the funnel walls to the periphery of the funnel mouth, resulting in a temperature gradient *along* the interface from the periphery to the funnel centerline, could not be eliminated [21]. The thermal conductivity of stainless steel is ~78 times that of PMMA, the funnel designs were similar, and the temperatures at the funnel throats were very nearly the same in all experiments. If this hypothesis is accepted, it leaves unanswered the question of how a Marangoni number of 27 847 could have existed in the experiments with the PMMA funnel without Marangoni convection having been initiated by the mechanism proposed by Pearson [22].

It is argued in [21] that since the heat transfer coefficient is an arbitrary coefficient in the Pearson model—there is no way within that model to determine its value [24]—and it can not be zero if the liquid is evaporating, the Pearson model only applies to nonvolatile liquids in semi-infinite containers. The experimental support for the Pearson model has been found only with nonvolatile liquids, primarily silicone oil [25–27]. Chai and Zhang [28] considered volatile liquids, and proposed a modification of the expression for the critical Marangoni number that had been proposed by Pearson. Barnes and colleagues [29,30] used interferometry to examine the temperature profile in water as it evaporated steadily under hydrodynamic conditions where Pearson's model indicated Marangoni convection would be present, but no evidence of Marangoni convection was found. Cammenga *et al.* [31] also measured the temperature profile near the interface of evaporating water under hydrodynamic conditions that Pearson's model would have suggested Marangoni convection should be present, but they did not find the evidence they expected. The existence of Marangoni convection in water was therefore questioned [32]. Since Marangoni convection in water has been clearly demonstrated [16,33], and the Pearson model is not strictly valid when evaporation is present, the relevant question is: under what conditions is Marangoni convection initiated when the liquid is evaporating?

Rosenblat *et al.* [34,35] considered a change in one of the parameters in the Pearson model. They took the system to have a finite aspect ratio (width over depth) but otherwise used an approximation similar to that of Pearson. They did not consider evaporation but allowed the liquid to be cooled using a heat transfer coefficient that they assigned arbitrary values. The side walls were taken to be adiabatic, but they were not then able to obtain an analytical solution with the no-slip boundary condition imposed at the walls. They introduced the "slippery" walls approximation, in which the fluid could not penetrate the walls, but could move parallel to them. Their prediction with these approximations was that as the aspect ratio is decreased, the critical Marangoni number is increased. The role of the aspect ratio in determining the stability of nonevaporating liquids was later investigated by several authors [36–38]. These investigators also used the "slippery side walls" approximation. Rather than use this approximation, we take the side walls to be isothermal and apply the no-slip condition at the walls.

Investigations of the effect of evaporation on the stability of a semi-infinite liquid layer have been made using the Hertz-Knudsen relation and assuming the interfacial temperatures of the liquid and vapor phases have the same value [39–42]. When the Hertz-Knudsen relation is adopted, it is necessary to introduce the accommodation coefficient. This parameter has proven to be difficult to determine experimentally. An investigation of the values reported for it has indicated it varies by several orders of magnitude [9]. There is strong evidence that during evaporation the interfacial temperatures are discontinuous.

Margerit *et al.* [43] also used the Hertz-Knudsen relation to describe an evaporating, semi-infinite liquid film, but allowed the interfacial temperature to be discontinuous. Their approach introduces four parameters that were ultimately combined into an "equivalent" Biot number. They concluded that as the temperature discontinuity was increased the system became less stable, but evaporation has a stabilizing influence on the liquid. The value of the critical Marangoni number found in this approach appears to be approximately the same as those of Pearson. Thus, there would be no indication from this approach of how a Marangoni number of more than 27 000 could exist without initiating convection.

Prosperetti and Plesset considered the stability of a semi-infinite evaporating liquid layer [44] in which the energy transport through the vapor phase was neglected. As justification, they say: "*it is known* [45,46] that in the presence of

any appreciable evaporation flux the temperature gradient in the vapor is very nearly zero." When Refs. [45,46] are examined, no experimental evidence is found to support their claim. The evaporation of a thin film was considered by Burelbach *et al.* [47], and they also neglected the energy transport through the vapor in their analysis. A similar approach has been adopted in considering the evaporation of a sessile droplet [48,49]. In contrast, in [21], we described experiments with the stainless-steel funnel in which water evaporated with an average flux of 68 $\mathrm{mg/m^2\,s}$, and all of the energy to evaporate the liquid came through the vapor. When the evaporation flux was raised to 100 $\mathrm{mg/m^2\,s}$, the thermal conduction through the vapor was still more than that through the liquid: 133 compared with 117 $\mathrm{W/m^2}$.

In the model developed below, we impose the conservation-of-energy condition at the liquid-vapor interface, and take the energy transport from both phases into account. We examine the stability of a liquid layer with a finite aspect ratio that is heated from below and is evaporating into its vapor. We eliminate the heat transfer coefficient at the liquid-vapor interface by introducing the SRT expression for the evaporation flux. Importantly, the SRT expression for the evaporation flux does not contain any fitting parameters, and it has been examined experimentally [5,6,50]. When it is incorporated in a linear stability analysis quantitative predictions of the critical Marangoni number, Ma_c, can be made from knowledge of the interfacial conditions. When the proposed theory is used to examine the experiments with the stainless-steel funnel, it is predicted that the observed Marangoni convection was not initiated by a Pearson-type instability. For the experiments with the PMMA funnel, it is predicted that the experimental Marangoni number is less than the predicted critical value. Hence, no Marangoni convection is predicted for the PMMA funnel, even though the Marangoni number was greater than 27 000 and none was observed.

III. PROBLEM DEFINITION

Consider an incompressible, gravity-free liquid of uniform depth, δ, that is confined in a two-dimensional container with lateral isothermal side walls separated by a distance of $2L$. The fluid velocity, $\vec{V}(x,z,t)$, with component $U(x,z,t)$ in the x direction and $W(x,z,t)$ in the z direction, and the temperature, $T(x,z,t)$, must satisfy the following conditions at the boundaries:

$$\vec{V}(L,z,t) = \vec{V}(-L,z,t) = 0, \tag{1}$$

$$T(\pm L,z) = T_I^L, \tag{2}$$

where T_I^L is a constant and is equal to the temperature in the liquid at the interface before the system is subject to the perturbation,

$$T(x,\delta,0) = T_I^L. \tag{3}$$

At the bottom surface of the container

$$\vec{V}(x,0,t) = 0, \tag{4}$$

and the temperature at this position is constant, T_{th}, and has the same value for all values of x and t,

$$T(x,0,t) = T_{th}. \tag{5}$$

At the liquid-vapor interface, there is an evaporation flux, j_{ev}, and if the enthalpy on the vapor side of the interface is denoted h_I^V and that on the liquid side as h_I^L, then, if the temperature in both phases is uniform along the interface [17–20], conservation-of-energy gives

$$-\kappa^L(\nabla T)_{z=\delta}\cdot i_z + \kappa^V(\nabla T)_{z=\delta}\cdot i_z = j_{ev}(h_I^V - h_I^L), \tag{6}$$

where κ^L and κ^V are the thermal conductivities of the liquid and vapor phases, respectively. The change in enthalpies may be written in terms of the specific heats, c_p^L, c_p^V, evaluated at the triple point temperature, T_{tp}, and the latent heat at this point, h_{fg} [16]:

$$(h_I^V - h_I^L) = h_{fg}(T_{tp}) + c_p^V(T_I^V - T_{tp}) - c_p^L(T_I^L - T_{tp}), \tag{7}$$

where the interfacial-vapor temperature is denoted T_I^V.

The SRT expression for the evaporation flux [1,3,5,6,50,51] may be written in terms of the change in entropy that results from a molecule transferring from the liquid phase to the vapor phase, Δs_{LV}, and the equilibrium exchange rate between the liquid and vapor phases, K_e. If the chemical potentials of the molecules in the liquid and the vapor phases at the interface are denoted μ_I^L, μ_I^V, then the net rate of molecular flux from the liquid to the vapor phase is given by [5,52]

$$j_{ev} = 2K_e \sinh\left(\frac{\Delta s_{LV}}{k_b}\right), \tag{8}$$

where k_b is the Boltzmann constant, and Δs_{LV} may be written as

$$\Delta s_{LV} = \left(\frac{\mu_I^L}{T_I^L} - \frac{\mu_I^V}{T_I^V}\right) + h_I^V\left(\frac{1}{T_I^V} - \frac{1}{T_I^L}\right). \tag{9}$$

We assume the local equilibrium approximation is valid for the flat liquid-vapor interface that we consider, and apply statistical thermodynamics to determine the expressions for μ_I^V and h_I^V. Provided the isothermal compressibility κ_T and the saturation-vapor pressure, P_s, satisfies

$$\kappa_T|P^V - P_s| \ll 1,$$

for the triatomic water molecule, with the internal molecular vibration frequencies (phonons) denoted as ω_l, the expression for Δs_{LV} may be written as [3,5,52]

$$\frac{\Delta s_{LV}}{k_b} = 4\left(1 - \frac{T_I^V}{T_I^L}\right) + \left(\frac{1}{T_I^V} - \frac{1}{T_I^L}\right)\sum_{l=1}^{3}\left(\frac{\hbar\omega_l}{2k_b} + \frac{\hbar\omega_l}{k_b[\exp(\hbar\omega_l/k_bT_I^V) - 1]}\right) + \frac{v_f}{k_bT_I^L}[P_I - P_s(T_I^L)] + \ln\left[\left(\frac{T_I^V}{T_I^L}\right)^4\left(\frac{P_s(T_I^L)}{P_I^V}\right)\right] + \ln\left(\frac{q_{vib}(T_I^V)}{q_{vib}(T_I^L)}\right), \tag{10}$$

$$q_{vib}(T) \equiv \prod_{l=1}^{3} \frac{\exp(-\hbar\omega_l/2k_bT)}{1-\exp(-\hbar\omega_l/k_bT)}, \tag{11}$$

and

$$K_e = \frac{P_s(T_I^L)\exp[(v_f/v_g)(P_I/P_s(T_I^L)-1)]}{\sqrt{2\pi m_w k_b T_I^L}}, \tag{12}$$

where v_f is the molecular specific volume, m_w is the molecular weight of the fluid, and P_I is the pressure in the liquid and vapor phases at the interface.

When Eqs. (10) and (12) are combined with Eq. (8), one obtains an expression for the evaporation flux that is in terms of the instantaneous interfacial properties T_I^L, T_I^V, P_I, the material properties of water $P_s(T_I^L)$, v_f, and the molecular phonons of the water molecule, ω_l. We take the material properties and the internal molecular vibration frequencies to be known from previous, independent experiments. Note that there are no free or fitting parameters in the SRT equation for the evaporation flux.

Conservation of mass in the liquid film gives

$$\frac{\partial\delta}{\partial t} = [\vec{V}(x,0,t) - \vec{V}(x,\delta,t)] \cdot i_z, \tag{13}$$

and at the liquid-vapor interface

$$\vec{V}(x,\delta,t) \cdot i_z = v_f j_{ev}. \tag{14}$$

The liquid film is maintained of constant thickness by fluid entering the container uniformly at the bottom,

$$\vec{V}(x,0,t) \cdot i_z = v_f j_{ev}. \tag{15}$$

Thus, as seen from Eq. (13), $\delta(t)$ is constant, an approximation that is consistent with recent experimental observation [53].

If γ_T denotes the change in surface tension with temperature and η the dynamic viscosity, a stress balance at the interface requires

$$\eta\left(\frac{\partial U}{\partial z}\right)_{z=\delta} = \gamma_T\left(\frac{\partial T}{\partial x}\right)_{z=\delta}. \tag{16}$$

If the pressure is denoted as $P(x,z,t)$, the conservation of mass, linear momentum, and energy requires

$$\vec{\nabla}\cdot\vec{V} = 0, \tag{17}$$

$$\frac{\partial\vec{V}}{\partial t} + (\vec{V}\cdot\vec{\nabla})\vec{V} = -\frac{1}{\rho}\vec{\nabla}P + \nu\nabla^2\vec{V}, \tag{18}$$

$$\frac{\partial T}{\partial t} + (\vec{V}\cdot\vec{\nabla})T = \alpha\nabla^2 T, \tag{19}$$

where ν is the kinematic viscosity, ρ is the liquid density and α is the liquid thermal diffusivity. Viscous dissipation is neglected in Eq. (19) since we only consider an infinitesimal perturbation from the initial state in which there is no flow, but only energy transport by thermal conduction.

TABLE I. Experimental conditions and the calculated evaporation number, E_{ev}, and critical Marangoni number, Ma_{cf}, during water evaporation from a stainless-steel funnel [16,17,19].

Experimental conditions			
Expt.	EV6	EV7	EV8
Vap.-ph. press. (Pa)	786.6	783.9	777.3
Intf. vap. temp. (°C)	4.62	4.56	4.46
Intf. liq. temp. (°C)	3.56	3.47	3.35
Throat temp. (°C)	3.57	3.53	3.53
Average $-\kappa^L(\frac{\partial T^L}{\partial z})_{z=\delta}$ (W/m^2)	0	43.37	57.05
Average $\kappa^V(\frac{\partial T^V}{\partial z})_{z=\delta}$ (W/m^2)	158.09	121.83	145.16
δ (mm)	3.55	3.55	3.55
Ma_{exp}	10	127	447
Interface observed	quiescent	marginal	convective
Calculated value of E_{ev} and predicted critical Marangoni number, Ma_{cf}			
$E_{ev}\times 10^3$ (calculated using SRT)	0.5136	0.5173	0.5208
Ma_{cf} (A=0.15)	3.61×10^5	3.58×10^5	3.56×10^5

IV. EXPERIMENTAL OBSERVATIONS

In the experiments reported in [21], the evaporation took place either from a stainless steel or a PMMA funnel. The throat diameter in both cases was 1.09 mm, giving L a value of 0.54 mm. The funnel mouth was 3.55 mm above the throat, and we take this height to be the value of δ in each experiment. Thus, the aspect ratio, A, was 0.15 in these experiments. The experiments were performed under steady-state conditions and the measured temperatures on the funnel center lines at the liquid-vapor interface are listed in Tables I and II. Also, for each experiment, the interface was investigated for the presence of Marangoni convection (see Interface observed in Table I). The temperatures in these tables were used to calculate the experimental Marangoni numbers using the properties listed in the Appendix.

V. INITIAL STATE OF THE EVAPORATING LIQUID

At the initial time, we suppose the liquid is evaporating steadily, and is stably stratified. For water, this means the temperature at the interface is less than the ~3.5 °C throat temperature. At the highest evaporation rate, the Reynolds number of the flow entering the throat of the stainless-steel funnel was 5×10^{-5} and that for the PMMA funnel was 1.8×10^{-3}. Thus, we neglect the flow entering the funnels, and take the z component of the liquid velocity at the throat as approaching zero. At the liquid-vapor interface, the liquid speed perpendicular to the interface would be even smaller than that at the throat; thus we neglect the flow at this interface as well. As indicated by Eqs. (13)–(15), δ is constant in time, and that the initial state may be approximated as a steady conduction state with negligible convection,

TABLE II. Experimental conditions during water evaporation from a PMMA funnel [21], and the calculated values of the evaporation number, E_{ev}, and the critical Marangoni number when the system is approximated semi-infinite, $\mathrm{Ma}_{c\infty}$ and when it is approximated as finite, Ma_{cf}.

Experimental conditions					
Expt.	Expt. 1	Expt. 2	Expt. 3	Expt. 4	Expt. 5
Vap.-ph. press. (Pa)	631	459	403	231	209
Intf. vap. temp. (°C)	1.55	−2.52	−4.26	−10.25	−11.59
Intf. liq. temp. (°C)	0.50	−3.92	−6.02	−13.11	−14.75
Throat temp. (°C)	3.58	3.53	3.57	3.47	3.50
Avg. evap. flux ($\mathrm{mg/m^2\ s}$)	244	384	442	604	653
Average $-\kappa^L(\frac{\partial T^L}{\partial z})_{z=\delta}$ ($\mathrm{W/m^2}$)	315.39	574.49	653.99	993.10	1099.46
Average $\kappa^V(\frac{\partial T^V}{\partial z})_{z=\delta}$ ($\mathrm{W/m^2}$)	149.89	180.67	214.32	267.13	272.59
δ (mm)	3.55	3.55	3.55	3.55	3.55
Ma_{exp}	8277	17119	20326	27640	27847
Interface observed	quiescent	quiescent	quiescent	quiescent	quiescent
Calculated value of E_{ev} and predicted critical Marangoni numbers $\mathrm{Ma}_{c\infty}$ and Ma_{cf}					
$E_{ev}\times 10^3$ (calculated using SRT)	0.6112	0.7985	0.9390	1.484	1.473
$\mathrm{Ma}_{c\infty}$	55000	42000	38000	22000	22000
Ma_{cf} ($A=0.15$)	2.78×10^5	2.13×10^5	1.82×10^5	1.16×10^5	1.17×10^5

$$\vec{V}(x,z,0)=0, \tag{20}$$

and the temperature profile is given by

$$T^L(x,z,0)=T_{th}+\beta z. \tag{21}$$

If Eq. (21) is applied at the interface, where $T^L(x,\delta,0)=T_I^L$, the constant β may be determined

$$\beta=\frac{T_I^L-T_{th}}{\delta}. \tag{22}$$

Thus, β is expressed in terms of measurable quantities: the liquid film depth and the temperatures in the liquid at the liquid-vapor interface and at the bottom of the system.

Since gravity is not acting, $\vec{\nabla}P$ vanishes in the initial state [see Eq. (18)], and P is equal P_0, a constant. The initial state is the steady-state solution of the conservation equations. From Eqs. (6) and (7), conservation of energy at the interface becomes

$$j_{ev}^0(h_0^V-h_0^L)=-\kappa^L\beta+\kappa^V\left(\frac{\partial T^V}{\partial z}\right)_I, \tag{23}$$

where labeling a quantity with a 0 indicates it is to be evaluated at the initial time. We take the temperature gradient in the vapor as being time independent. Now we investigate the stability of the initial state by considering the result of subjecting it to a perturbation.

VI. LINEARIZATION OF THE GOVERNING EQUATIONS AND THEIR BOUNDARY CONDITIONS

We obtain the linearized governing equations from a perturbation analysis of the liquid phase, and assume the vapor phase is undisturbed. In the perturbed state, we take as the expression for the fluid velocity in the liquid phase

$$\vec{V}^L(x,z,t)=u(x,z,t)i_x+w(x,z,t)i_z, \tag{24}$$

the liquid phase pressure,

$$P^L=P_0+p(x,z,t), \tag{25}$$

and the liquid phase temperature

$$T^L=T_{th}+\beta z+\theta(x,z,t), \tag{26}$$

where $u(x,z,t)$, $w(x,z,t)$, $\theta(x,z,t)$, and $p(x,z,t)$ are the infinitesimal perturbations. The perturbed evaporation flux may be written as

$$j_{ev}=j_{ev}^0+\left(\frac{\partial j_{ev}}{\partial T^L}\right)_I\theta(x,\delta,t), \tag{27}$$

and the difference in the interfacial enthalpies may be expressed as

$$(h_I^V-h_I^L)=(h_0^V-h_0^L)-c_p^L\theta(x,\delta,t). \tag{28}$$

The expression for j_{ev} is given in Eqs. (8)–(12).

If Eqs. (13) and (17)–(19) are linearized by introducing the perturbations and nondimensionalized by scaling the length with δ, time with δ^2/ν, velocity with α/δ, pressure with $\rho\nu\alpha/\delta^2$ and temperature with $\beta\delta$, one finds

$$\nabla\cdot\vec{V}^L=0, \tag{29}$$

$$\frac{\partial\vec{V}^L}{\partial t}=\nabla p+\nabla^2\vec{V}^L, \tag{30}$$

$$\mathrm{Pr}\frac{\partial\theta}{\partial t} = \nabla^2\theta - \vec{V}^L \cdot i_z, \tag{31}$$

where Pr is the Prandtl number, ν/α.

We can eliminate the pressure term by taking the curl of Eq. (30) which yields the vorticity equation. After taking the curl of the vorticity equation and combining the result with the continuity equation, one finds [54]

$$\nabla^2\left(\frac{\partial}{\partial t} - \nabla^2\right)w = 0. \tag{32}$$

The linearized energy equation in the perturbed state may be written as

$$\left(\mathrm{Pr}\frac{\partial}{\partial t} - \nabla^2\right)\theta = -w. \tag{33}$$

At $z=0$, we assume the perturbation vanishes

$$w(x,0,t) = 0, \tag{34}$$

and since $u(x,0,t)$ vanishes for all values of x, so does

$$\left(\frac{\partial u}{\partial x}\right)_{z=0} = 0. \tag{35}$$

Then from continuity

$$\left(\frac{\partial w}{\partial z}\right)_{z=0} = 0. \tag{36}$$

If the aspect ratio, A, is defined as L/δ, then on the isothermal side walls, $x=\pm A$, one finds from Eqs. (2) and (26)

$$\theta(\pm A,z,t) = 0. \tag{37}$$

Similarly, from Eqs. (1) and (24),

$$w(\pm A,z,t) = 0. \tag{38}$$

We write the solution to the continuity equation in terms of the stream function ψ,

$$w = -\frac{\partial\psi}{\partial x}, \tag{39}$$

and

$$u = \frac{\partial\psi}{\partial z}, \tag{40}$$

then Eq. (1) gives

$$\left(\frac{\partial\psi}{\partial z}\right)_{x=\pm A} = \left(\frac{\partial\psi}{\partial x}\right)_{x=\pm A} = 0. \tag{41}$$

Thus, ψ is a constant and we take the constant to be 0,

$$\psi(\pm A,z,t) = 0. \tag{42}$$

Since T has the value T_{th} at $z=0$, as seen from Eq. (26), the temperature perturbation also vanishes there,

$$\theta(x,0,t) = 0. \tag{43}$$

For the evaporation fluxes before the onset of convection, one finds from Eqs. (13)–(15) that for δ to remain constant

$$w(x,1,t) = 0. \tag{44}$$

From Eqs. (16) and (29)

$$\left(\frac{\partial^2 w}{\partial z^2}\right)_{z=1} = -\mathrm{Ma}\left(\frac{\partial^2\theta}{\partial x^2}\right)_{z=1}, \tag{45}$$

where the Marangoni number Ma is given by

$$\mathrm{Ma} = \frac{\gamma_T\beta\delta^2}{\eta\alpha}. \tag{46}$$

After substituting Eqs. (27) and (28) into Eqs. (6) and (7), linearizing, and nondimensionalizing, the-conservation-of-energy equation becomes

$$E_{ev}\left(\frac{\partial\theta}{\partial z}\right)_{z=1} + \theta(x,1,t) = 0, \tag{47}$$

where the evaporation number E_{ev}, is defined

$$E_{ev} = \frac{\kappa^L}{\delta}\left[(h_0^V - h_0^L)\left(\frac{\partial j_{ev}}{\partial T^L}\right)_I - c_p^L j_{ev}^0\right]^{-1}. \tag{48}$$

We note that E_{ev} may be evaluated for the given instantaneous interfacial properties (T_I^L, T_I^V, P_I) using SRT, Eqs. (8)–(12), and the liquid-layer thickness. Thus, there is no need to introduce a phenomenological heat transfer coefficient [55,56] into the analysis.

A. Conditions for marginal stability of a finite-sized system

We suppose $w(x,z,t)$ and $\theta(x,z,t)$ to be of the form

$$w(x,z,t) = -w_s(x,z)\exp(\sigma t),$$

$$\theta(x,z,t) = \theta_s(x,z)\exp(\sigma t), \tag{49}$$

where σ is the growth rate and is in general complex. Then

$$\frac{\partial w}{\partial t} = -w_s\sigma\exp(\sigma t),$$

$$\frac{\partial\theta}{\partial t} = \theta_s\sigma\exp(\sigma t). \tag{50}$$

As indicated by Eq. (20), in the initial state w_s is equal zero, but now we wish to determine the expression for w_s and θ_s in the state of marginal stability. This state exists when $\mathrm{Re}(\sigma)$ vanishes. We will show that when this state is reached $\mathrm{Im}(\sigma)$ is also zero, indicating the marginally stable state is stationary in time [57–59] for the finite aspect ratio problem defined in the previous section.

When $w(x,z,t)$ and $\theta(x,z,t)$ are substituted into Eqs. (32) and (33), one finds

$$\sigma\nabla^2 w_s - \nabla^4 w_s = 0,$$

$$\sigma\,\mathrm{Pr}\;\theta_s - \nabla^2\theta_s = w_s. \tag{51}$$

If the real and imaginary portions of Eq. (51) are considered separately, one finds

$$\mathrm{Re}(\sigma)\nabla^2 w_s - \nabla^4 w_s = 0, \tag{52}$$

$$\mathrm{Im}(\sigma)\nabla^2 w_s = 0, \tag{53}$$

$$\mathrm{Re}(\sigma)\mathrm{Pr}\ \theta_s - \nabla^2\theta_s = w_s, \tag{54}$$

$$\mathrm{Im}(\sigma)\mathrm{Pr}\ \theta_s = 0. \tag{55}$$

Since in the marginally stable state, by definition, $\mathrm{Re}(\sigma)$ vanishes

$$\left(\frac{\partial^2}{\partial x^2} + \frac{\partial^2}{\partial z^2}\right)\left(\frac{\partial^2}{\partial x^2} + \frac{\partial^2}{\partial z^2}\right) w_s = 0, \tag{56}$$

and

$$\left(\frac{\partial^2}{\partial x^2} + \frac{\partial^2}{\partial z^2}\right)\theta_s = -w_s. \tag{57}$$

It will be shown below that for Eqs. (53) and (55) to be satisfied, $\mathrm{Im}(\sigma)$ must vanish; thus, Eqs. (56) and (57) must be solved to determine w_s and θ_s in the marginally stable state.

The boundary conditions in the marginally stable state at $x = \pm A$ are

$$w_s(\pm A, z) = 0; \tag{58}$$

and since

$$w_s = -\frac{\partial \psi_s}{\partial x},$$

and

$$u_s = \frac{\partial \psi_s}{\partial z},$$

from Eqs. (37) and (42), we have at $x = \pm A$,

$$\theta_s(\pm A, z) = 0, \tag{59}$$

$$\psi_s(\pm A, z) = 0. \tag{60}$$

At $z=0$, the boundary conditions, Eqs. (34), (36), and (43), give

$$w_s(x,0) = \left(\frac{\partial w_s}{\partial z}\right)_{z=0} = 0, \tag{61}$$

$$\theta_s(x,0) = 0. \tag{62}$$

And at $z=1$, one finds from Eqs. (44), (45), (47), and (50) that in the marginally stable state

$$w_s(x,1) = 0, \tag{63}$$

$$\left(\frac{\partial^2 w_s}{\partial z^2}\right)_{z=1} = \mathrm{Ma}\left(\frac{\partial^2 \theta_s}{\partial x^2}\right)_{z=1}, \tag{64}$$

$$E_{\mathrm{ev}}\left(\frac{\partial \theta_s}{\partial z}\right)_{z=1} + \theta_s(x,1) = 0. \tag{65}$$

For the system to be marginally stable, one condition that the velocity perturbation in the z direction must satisfy is given by the biharmonic equation [Eq. (56)]. The corresponding condition that the temperature perturbation must satisfy may be seen in Eq. (57). The boundary conditions for these perturbations are listed in Eqs. (58)–(65).

B. Conditions for marginal stability of a system that is infinite in the horizontal direction

For comparison with the results obtained when the system is finite, we first consider a system with infinite aspect ratio (i.e., $A \to \infty$). Following the procedure outlined above, one is again led to Eqs. (56) and (57), but the boundary conditions are now different. There is no longer an eigenvalue problem in the horizontal direction. We suppose the solution is periodic in this direction with wave number k,

$$w_s = f(z)\cos(kx), \tag{66}$$

and that

$$\theta_s = g(z)\cos(kx). \tag{67}$$

Substituting the forms of w_s and θ_s into Eqs. (56) and (57) gives

$$(D^2 - k^2)^2 f(z) = 0, \tag{68}$$

and

$$(D^2 - k^2) g(z) = -f(z). \tag{69}$$

At $z=0$, Eqs. (34), (36), and (43) now give

$$f(0) = \left(\frac{\partial f}{\partial z}\right)_{z=0} = 0, \tag{70}$$

$$g(0) = 0. \tag{71}$$

And at $z=1$, one now finds from Eqs. (44), (45), and (47)

$$f(1) = 0, \tag{72}$$

$$\left(\frac{\partial^2 f}{\partial z^2}\right)_{z=1} = -\mathrm{Ma}_\infty k^2 g(1), \tag{73}$$

$$E_{ev}\left(\frac{\partial g}{\partial z}\right)_{z=1} + g(1) = 0. \tag{74}$$

The problem thus reduces to the solution of ordinary differential equations and once the solution is available, the Marangoni number can be obtained from Eq. (73),

$$\mathrm{Ma}_\infty = \frac{a[(k^2 - 2K)k\cosh(k) + (1-K)k^2\sinh(k)]}{g(1)k^2}, \tag{75}$$

where

$$K = \frac{k\cosh(k) - \sinh(k)}{\sinh(k)}, \tag{76}$$

and after simplification $g(1)$ is given by

$$g(1) = a\frac{E_{ev}(-k^3\coth(k) + (\sinh(k))^2)}{4k^2(E_{ev}k\cosh(k) + \sinh(k))}. \tag{77}$$

Note that the arbitrary constant a divides out in the final expression for the Marangoni number.

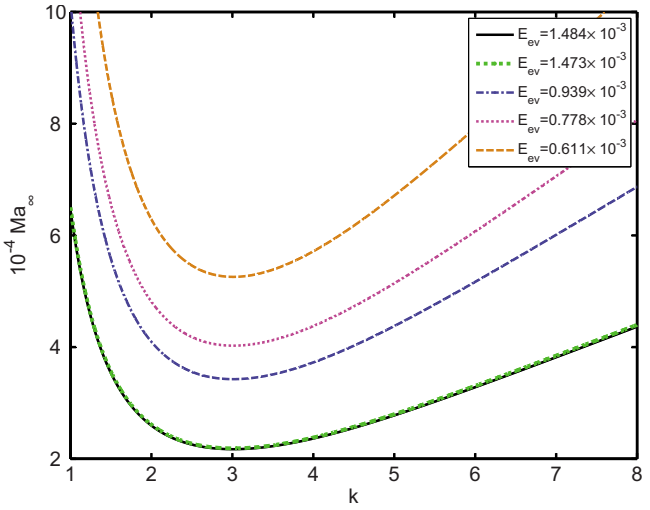

FIG. 1. (Color online) For a semi-infinite liquid film, the Marangoni number is plotted as a function of the evaporation number, E_{ev}.

As seen in Eqs. (75)–(77), Ma_∞ depends on two parameters, E_{ev} and the wave number k. In Fig. 1, for the experimental values of E_{ev} listed in Table II, Ma_∞ is shown as a function of the wave number. The most unstable mode, k_c, for each value of E_{ev} corresponds to $k_c = \sim 3$. For the most unstable mode, as observed in Fig. 1, the critical value of the Marangoni number, $\mathrm{Ma}_{c\infty}$, is determined by the value of E_{ev}, and as E_{ev} is increased $\mathrm{Ma}_{c\infty}$ is decreased. In Table II, it is seen that as E_{ev} is increased, the evaporation flux increases. Thus, the prediction is that evaporation destabilizes the system in the sense that evaporation reduces the critical Marangoni number.

In the experiments conducted with the PMMA funnel (Table II), the evaporation flux was progressively raised. For a semi-infinite liquid that had the measured values of T_I^L, T_I^V, and P at the interface, the calculated value of the critical Marangoni number, $\mathrm{Ma}_{c\infty}$, is listed, along with the calculated value of the Marangoni number for each experiment, Ma_{exp}. Note that for the experiments with the lower evaporation fluxes (experiments 1–3) $\mathrm{Ma}_{c\infty} > \mathrm{Ma}_{exp}$. Thus, for these experiments the prediction is that there would be no transition from a quiescent to a convecting interface, but if the liquid were approximated as semi-infinite, in experiments 4 and 5, $\mathrm{Ma}_{c\infty} < \mathrm{Ma}_{exp}$. Thus, the prediction is that if the liquid film were semi-infinite, Marangoni convection would have occurred in experiments 4 and 5. However, Marangoni convection was not observed in these cases either, as indicated by the last line of the experimental conditions (Table II). This suggests that the finite size of the liquid phase was important for these two experiments.

VII. EXPRESSION FOR w_s FOR A MARGINALLY STABLE SYSTEM THAT HAS A FINITE ASPECT RATIO

For a system with a finite aspect ratio, the solution to Eq. (56) may be expressed as

$$w_s = \sum_{n=1}^{\infty} [\sinh k_n z + K_n z \sinh k_n z - k_n z \cosh k_n z] \times (C_n \sin k_n x + D_n \cos k_n x), \tag{78}$$

where C_n and D_n are arbitrary constants, and

$$k_n \equiv n\pi/A, \tag{79}$$

and

$$K_n \equiv \frac{k_n \cosh k_n - \sinh k_n}{\sinh k_n}. \tag{80}$$

The no-slip boundary conditions that we consider are given in Eqs. (58) and (60). The conditions at the liquid-vapor interface and at the heating surface are given in Eqs. (60) and (61). For the system that we consider, D_n vanishes, but we note that if slip were allowed at $x = \pm A$ [34,36–38], D_n would be nonzero, and the cos k_n modes would be the only ones present. One may verify that w_s with $D_n = 0$ is the exact solution for the biharmonic equation with the boundary conditions given in Eqs. (58), (60), (61), and (63).

Since we now have the expression for w_s, Eq. (78), we can complete the proof that the marginally stable state is stationary. From the expression for w_s, one finds

$$\nabla^2 w_s \neq 0;$$

thus, from Eq. (53),

$$\mathrm{Im}(\sigma) = 0.$$

Hence, the marginally stable state is stationary in time since both $\mathrm{Re}(\sigma)$ and $\mathrm{Im}(\sigma)$ vanish.

From the definition of the stream function, one finds for each mode

$$w_s^n = -\partial \psi_s^n / \partial x.$$

If w_s^n is integrated, first from $-A$ to x and then from A to x, since $\psi^n(\pm A, z) = 0$, one finds

$$\psi_s^n = -\int_{-A}^{x} w_s^n(x', z)dx' = -\int_{A}^{x} w_s^n(x', z)dx'. \tag{81}$$

Also, by integrating the continuity equation and applying the boundary conditions given in Eq. (60)

$$u_s^n(x,z) = -\int_A^x \frac{\partial w_s^n}{\partial z}(x', z)dx' = -\int_{-A}^{x} \frac{\partial w_s^n}{\partial z}(x', z)dx'. \tag{82}$$

Note that the expression for u_s^n may be constructed from the expression for w_s^n. From Eqs. (78) and (82), one finds

$$u_s^n(x,z) = \frac{C_n}{k_n}(\cos n\pi - \cos k_n x)((K_n - k_n^2 z)\sinh k_n z + K_n k_n z \cosh k_n z). \tag{83}$$

Note $u_s^n(x,z)$ is an even function of x, and at $z = 1$, the direction of the flow is determined by the sign of $((-1)^n - \cos k_n x)$. For $-A < x < A$, the sign of this term is determined by the sign of $(-1)^n$. Thus, for each mode, the surface flow is

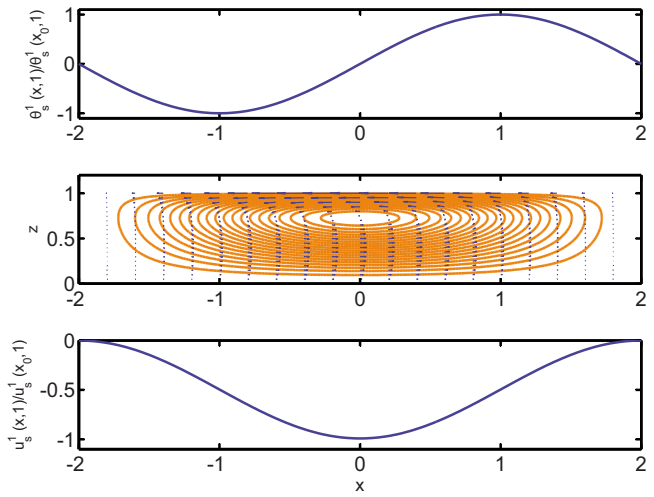

FIG. 2. (Color online) For an aspect ratio of 2, an E_{ev} value of 1.473×10^{-3}, and the first mode, the scaled temperature perturbation at the top surface is shown in the upper graph, the calculated streamlines for this mode are shown in the middle graph, and the surface speed is shown in the lower graph.

unidirectional, but the direction changes for successive modes. Using the data in Table II corresponding to the highest value of Ma_{exp}, experiment 5, this behavior is demonstrated in Figs. 2–4 and has not been previously predicted. This mode was obtained from the new expression for the z component of the perturbed velocity [Eq. (78)].

As may be seen from Eqs. (78) and (83) for $x=0, w_s(0,z)$ is zero for all modes, but $u_s^n(0,z)$ is zero only for the even modes. Thus, as indicated in Fig. 2 for an even mode, the centerline is a stagnation line. Apart from the stagnation lines, the other positions where both w_s^n and u_s^n vanish are at the center of the rolls.

For a given A and n, the value of k_n can be determined from Eq. (79) and the positions, z_i, where $u_s^n(x,z_i)$ vanishes may be obtained from Eq. (83) for any x,

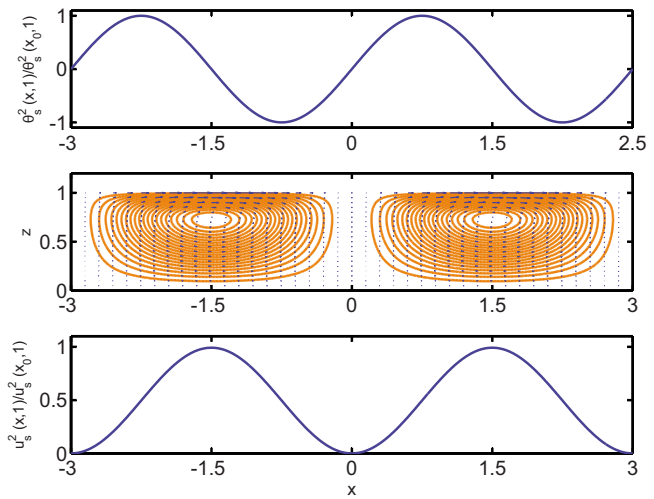

FIG. 3. (Color online) For an aspect ratio of 3, an E_{ev} value of 1.473×10^{-3}, and the second mode, the scaled temperature perturbation at the top surface is shown in the upper graph, the calculated streamlines for this mode are shown in the middle graph, and the surface speed is shown in the lower graph.

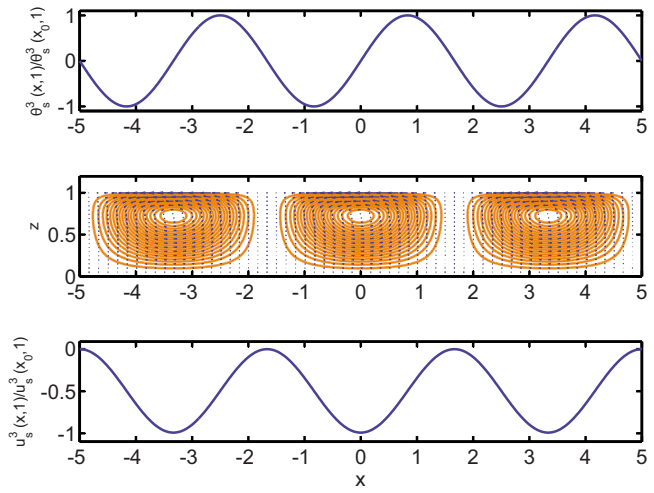

FIG. 4. (Color online) For an aspect ratio of 5, an E_{ev} value of 1.473×10^{-3}, and the third mode, the scaled temperature perturbation at the top surface is shown in the upper graph, the calculated streamlines for this mode are shown in the middle graph, and the surface speed is shown in the lower graph.

$$\tanh(k_n z_i) = \frac{K_n k_n z_i}{k_n{}^2 z_i - K_n}. \tag{84}$$

The values of x_i where both u_s^n and w_s^n vanish may be determined from Eq. (78). Since

$$\sinh(k_n z_i) + K_n z_i \sinh(k_n z_i) - k_n z_i \cosh(k_n z_i) \neq 0,$$

x_i is obtained from

$$\sin(k_n x_i) = 0. \tag{85}$$

At the positions other than the stagnation lines where $u_s^n(x_i,z_i)$ and $w_s^n(x_i,z_i)$ vanish are illustrated in Figs. 2–4 as the roll centers. The values of x_i and z_i corresponding to the roll centers calculated by the outlined procedure are listed in Table III. If the boundary condition at the side walls had required slip, then w_s would have been expressed in terms of $\cos k_n x$ modes. These modes do not exhibit unidirectional surface flow [34].

The expression for ψ_s^n may be obtained from Eq. (81),

$$\psi_s^n(x,z) = \frac{C_n}{k_n}(\cos n\pi - \cos k_n x) \times (k_n z \cosh k_n z - (1 + K_n z \sinh k_n z)). \tag{86}$$

The position on the liquid-gas interface where u_s^n has its maximum value, x_0, may be determined from

TABLE III. Positions of roll centers.

$n=1, A=2$	$u_s=w_s=0$	(x_1,z_1)		
		(0,0.68)		
$n=2, A=3$	$u_s=w_s=0$	(x_1,z_1)	(x_2,z_2)	
		$(-1.5,0.68)$	(1.5, 0.68)	
$n=3, A=5$	$u_s=w_s=0$	(x_1,z_1)	(x_2,z_2)	(x_3,z_3)
		$(-3.33,0.68)$	(0, 0.68)	(3.33, 0.68)

$$\left(\frac{\partial u_s^n(x,1)}{\partial x}\right)_{x=x_0} = 0. \tag{87}$$

Then

$$u_s^{n\,max} = u_s^n(x_0,1).$$

The speeds may now be scaled in terms of $u_s^{n\,max}$ and the constant C_n eliminated. As seen in Figs. 2–4, the x-component of velocity, u_s, (lower panel) is symmetric about x equal to zero, but the flow at $z=1$ is unidirectional.

VIII. EXPRESSION FOR θ_s IN THE STATE OF MARGINAL STABILITY

The expression for the temperature perturbation θ_s must satisfy Eq. (57) and the corresponding boundary conditions Eqs. (60), (62), and (65). We choose to represent θ_s in a sine series,

$$\theta_s = \sum_{l=1}^{\infty} C_l g_l(z) \sin k_l x, \tag{88}$$

where C_l are the coefficients of the expansion. Note that θ_s satisfies the isothermal boundary conditions at the sidewalls. Moreover each mode of θ_s corresponds to a mode of w_s since the latter is also a sine series. Note that w_s and θ_s are related through Eq. (57).

This choice of θ_s and the expression of w_s from Eq. (78) are inserted into Eq. (57) to yield

$$\sum_{l=1}^{\infty} C_l \left[\frac{d^2 g_l}{dz^2} - k_l^2 g_l\right] \sin k_l x = -\sum_{m=1}^{\infty} C_m [\sinh k_m z + K_m z \sinh k_m z - k_m z \cosh k_m z] \sin k_m x. \tag{89}$$

After multiplying both sides by $\sin(n\pi x/A)$ and integrating over x from $x=-A$ to $x=+A$, one obtains,

$$\left(\frac{d^2 g_n}{dz^2} - k_n^2 g_n\right) = -[\sinh(k_n z) + K_n z \sinh(k_n z) - k_n z \cosh(k_n z)]. \tag{90}$$

The general solution of the Eq. (90) may now be written as

$$g_n(z) = \bar{C}_1 \cosh(k_n z) + \bar{C}_2 \sinh(k_n z) - \frac{K_n}{4k_n^2}(k_n z^2 \cosh(k_n z) - z \sinh(k_n z)) + \frac{1}{4k_n}(k_n z^2 \sinh(k_n z) - 3z \cosh(k_n z)). \tag{91}$$

When this expression for θ_s is required to satisfy the boundary conditions at the top and bottom surfaces,

$$g_n(0) = 0,$$

$$E_{ev}\frac{dg_n}{dz}(1) = -g_n(1), \tag{92}$$

one obtains $\bar{C}_1 = 0$ and

$$\bar{C}_2 = \frac{1}{4k_n^2(k_n E_{ev}\cosh(k_n) + \sinh(k_n))}[E_{ev}(k_n K_n \cosh(k_n) + k_n^2 K_n \sinh(k_n) - K_n \sinh(k_n) + k_n^2 \sinh(k_n) - k_n^3 \cosh(k_n) + 3k_n \cosh(k_n)) + (k_n K_n \cosh(k_n) - K_n \sinh(k_n) - k_n^2 \sinh(k_n) + 3k_n \cosh(k))]. \tag{93}$$

Thus, the expression for θ_s has now been obtained in terms of the parameters E_{ev} and A. The value of E_{ev} was calculated from the experimental results listed in Table II using Eq. (48). The values of A for each case are given in the captions of Figs. 2–4. The temperature perturbation at the interface is shown in the upper panel of each of these figures. Note that for the second mode, Fig. 2, the temperature gradient *alone* near the side walls does not determine the direction of the surface velocity. The viscous effects arising from the side walls have an influence on the direction of the surface flow. For the second mode, Fig. 2, in the core of the fluid, the reversal of the temperature gradient, results in a stagnation point of the flow at the centerline. There are, however, two stagnation points for the third mode (Fig. 4). An investigation indicates the number of stagnation points depends on the mode. For the n^{th} mode, $n-1$ stagnation points are predicted in the flow.

IX. CRITICAL MARANGONI NUMBER FOR FINITE-SIZED SYSTEMS

The critical Marangoni number for a finite-sized system is determined from the only boundary condition that has not yet been satisfied. For this type of system, Eq. (64), the tangential stress boundary condition at the interface ($z=1$) for each mode may be expressed as

$$\frac{\partial^2 w_s^n}{\partial z^2} = \mathrm{Ma}_n \frac{\partial^2 \theta_s^n}{\partial x^2}, \tag{94}$$

The expression for w_s^n is given in Eq. (78) and the expression for θ_s^n in Eqs. (88)–(93). After putting these expressions into Eq. (94), one finds

$$\mathrm{Ma}_n = \frac{[(k_n^2 - 2K_n)k_n \cosh(k_n) + (1-K_n)k_n^2 \sinh(k_n)]}{g_n(1)k_n^2}. \tag{95}$$

Using this expression, calculating the value E_{ev} for experiment 5 of Table II, choosing a mode (or value of n), Ma may be plotted as a function of the aspect ratio A. The type of results found is illustrated in Fig. 5 for the first eight modes. The horizontal dashed line in this figure indicates the value of the critical Marangoni number obtained for a semi-infinite liquid layer when E_{ev} has a value of 1.473×10^{-3} (see Fig.

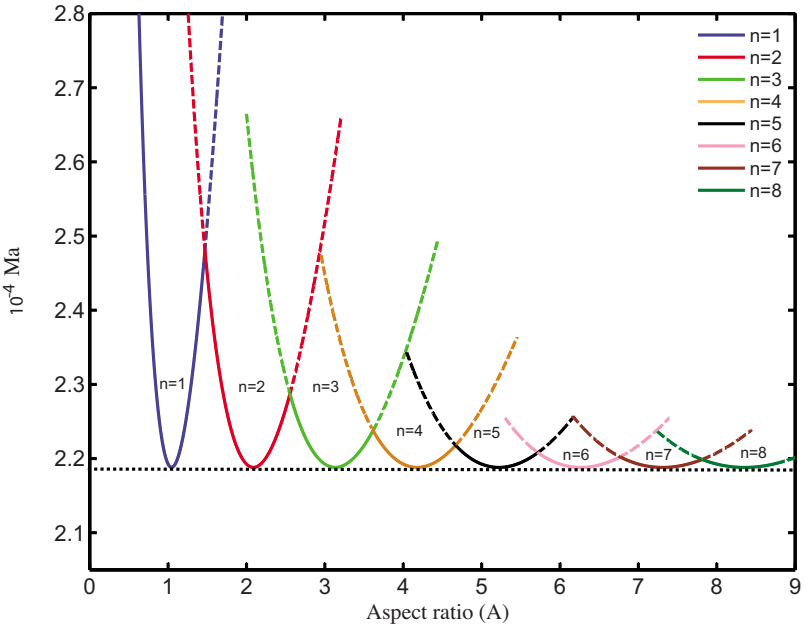

FIG. 5. (Color online) When the interfacial evaporation number, E_{ev}, is 1.473×10^{-3}, the horizontal dashed line indicates the critical Marangoni number for a semi-infinite system. The Marangoni numbers for the first eight modes of a finite-sized system are shown as a function of A. Note that for certain values of A the critical values of the Marangoni number is the same as that for a semi-infinite system.

1). Note that at certain values of the aspect ratios, A, the critical Marangoni number for the finite system, Ma_{cf}, is equal to that for the semi-infinite system $\mathrm{Ma}_{c\infty}$. This occurs when A is such that the critical wave number of the horizontal motion, $k_n=n\pi/A$, is equal to that of the semi-infinite system, k_c, for that value of E_{ev}. We denote this value of the aspect ratio as A_∞. For the experiments described in Table II, $k_c\simeq3$. The value of A_∞ may, in general, be written as

$$k_c = k_n.$$

$$A_\infty = \frac{n\pi}{k_c}. \tag{96}$$

When $A>A_\infty$ or $A<A_\infty$, the system is stabilized compared to that when $A=A_\infty$. For the funnel used for the experiments described in Table II, A is approximately 0.15. For this value of A and the values of E_{ev} calculated for experiments 4 and 5 of this table, the value of Ma_{cf} is greater than Ma_{exp}; thus the transition from quiescent to a convecting interface is not predicted for these experiments either.

At certain values of A, two modes are equally unstable, and there is the possibility of mode switching, as has been observed experimentally by Johnson and Narayanan [60]. As indicated in Figs. 2–4, a change in the mode changes the flow pattern.

X. DISCUSSION AND CONCLUSION

A linear stability analysis has been performed to determine the conditions under which an evaporating liquid layer of thickness δ heated from below is marginally stable. Both an infinite and finite values of the aspect ratio are considered. When the liquid evaporates, the interface can be heated both through the liquid and through the vapor phases. For finite aspect ratio systems, the liquid is taken to be held in a two-dimensional container that has isothermal side walls. The fundamental difference between the proposed approach and earlier ones is that for both finite and semi-infinite systems, statistical rate theory is applied at the liquid-vapor interface to predict the evaporation flux [Eqs. (8)–(12)]. This removes the necessity of introducing phenomenological coefficients such as the heat transfer coefficient [56] or the accommodation coefficient [9] or the Onsager coefficients [43]. The expression obtained for the evaporation flux from SRT [5] has significant experimental support [6,50], and allows the interfacial temperatures and chemical potentials to be discontinuous. The temperature in the vapor at the interface has been found experimentally to be greater than that of the liquid [1–4,16–19,50,61–63] and this disequilibrium at the interface is included in the SRT calculation of the evaporation flux.

The steady-state solution of the coupled system of equations is perturbed by considering small changes in the interfacial-liquid temperature. For both finite and semi-infinite systems, this leads to the boundary condition given in Eq. (47) that contains the evaporation number, E_{ev}. Using SRT, Eqs. (8)–(12), the value of this parameter may be determined from values of the instantaneous interfacial properties, T_I^L, T_I^V, P and the liquid-layer thickness, δ. There are no fitting or undefined parameters in this procedure; thus, the value of E_{ev} may be calculated for a given physical circumstance. If the conditions at the interface are changed so as to increase the value of E_{ev}, the total-energy flux to the interface increases, as does the average evaporation flux (see Table II).

When the aspect ratio is taken to be infinite and the solution of the linearized equations is assumed to be periodic in the horizontal direction with wave number k, the Marangoni number Ma_∞ depends on k and E_{ev}. For each value of E_{ev}, there is a critical value of k, denoted k_c. This case is depicted in Fig. 1. Note that for the range E_{ev} values considered in the experiments, as E_{ev} is increased, $\mathrm{Ma}_{c\infty}$ decreases; thus, for these experimental conditions, evaporation is predicted to destabilize even the semi-infinite system.

The opposite effect of evaporation on the stability of semi-infinite systems was predicted by Margerit *et al.* [43]. They used nonequilibrium thermodynamics and a linearized-Hertz-Knudsen expression for the evaporation flux. The thermodynamic forces were taken to be the interfacial-temperature discontinuity and the deviation of the liquid-interface temperature from the saturation value. They concluded the interfacial-temperature discontinuity destabilizes the system, but the deviation of the interfacial-liquid temperature from the saturation temperature (Hertz-Knudsen-evaporation flux) had a stabilizing effect on the system. When SRT is applied both the interfacial-temperature discontinuity and the deviation from equilibrium are included in the value of E_{ev}, and one predicts the net effect of the evaporation.

In Ref. [21], it is argued that the Pearson model does not apply when the liquid evaporates because: (1) at the liquid-vapor interface, energy conservation is not satisfied. For example, the latent heat plays no role in that model. (2) Also, the temperature discontinuity that he assumed is in the opposite direction of that found in the experiments. (3) The value of the Marangoni number that is predicted to be critical is much smaller than those observed in the experiments with the PMMA funnel.

For a finite-sized system, the predictions are more complex: consider a finite-sized and a semi-infinite layer of the same liquid. For isothermal side walls and the no-slip conditions at all walls, a separation-of-variables type solution is obtained in which each mode depends on the aspect ratio, A, and E_{ev}. Remarkable new modes are predicted (Figs. 2–4) : for each mode, the surface flow is unidirectional, but the direction is predicted to change with successive modes. For evenly numbered modes, there is a flow stagnation point on the center line of the container. In general, flow rolls are present in the bulk liquid, and the number of rolls depends on the flow mode. Because of viscous effects at the side walls, on the liquid-vapor interface, there is a portion of the interface where the flow direction is different than that expected from the predicted temperature gradient: the flow is in the direction of increasing temperature. For example, as indicated in Fig. 2, the prediction is that the flow must be some distance away from the viscous effects of the side walls before the flow direction is controlled by the temperature gradient. Under certain conditions the finite and semi-infinite systems are predicted to have the same value of their critical Marangoni numbers. If the same conditions exist at the interface (T_I^L, T_I^V, P) and the liquid layers have the same thickness, then they would have the same value of E_{ev}. If the finite-sized system had aspect ratios of $n\pi/k_c$, denoted A_∞, the wave length in the horizontal direction in the two systems would be the same. This circumstance is depicted in Fig. 5. Thus, for a finite-sized system with one of these aspect ratios, the aspect ratio plays no role in determining the critical Marangoni number: $\mathrm{Ma}_{cf}=\mathrm{Ma}_{c\infty}$. However, if the aspect ratio is either greater or less than A_∞, the effect is predicted to stabilize the system because the critical value of the Marangoni number is increased for these values of A. The amount of the increase depends on the value of E_{ev} and the mode. An example for one value of E_{ev} and several modes is given in Fig. 5.

For the experiments described in Table II, the value of E_{ev} was determined from the measured values of T_I^L, T_I^V, P, δ, and A in each experiment was less than A_∞. The predicted value of Ma_{cf} is listed in the Table. Note that for each experiment, $\mathrm{Ma}_{cf} > \mathrm{Ma}_{exp}$. Since the liquid was stably stratified, the Rayleigh number would be negative, and the Nield model would indicate the critical Marangoni number would be even larger than Ma_{cf} [21,23]. Thus, no transition to Marangoni convection is predicted for any of the water evaporation experiments described in Table II, and none were observed: the interface was observed to be quiescent in each experiment. This supports the hypothesis of [21] suggesting that the Marangoni convection observed in the experiments with the stainless-steel funnel, Table I, resulted from thermal conduction in the funnel walls imposing a temperature gradient along the liquid-vapor interface rather than from an instability.

ACKNOWLEDGMENTS

We wish to acknowledge the support of the Canadian and European Space Agencies and the Natural Sciences and Engineering Research Council of Canada.

APPENDIX

The correlations used to calculate water properties (in SI units, T in °C) are listed below. The density was taken to be [64]

$$\rho(T) = 999.867\,876\,9 + 0.068\,252\,345\,12T - 0.009\,172\,478\,57T^2 + 0.000\,108\,280\,32T^3 - 0.172\,307\,755\,6\times 10^{(-5)}T^4 + 0.438\,663\,578\,8\times 10^{(-7)}T^5 - 0.956\,189\,531\,5\times 10^{(-9)}T^6, \quad \text{(A1)}$$

the surface tension [65]

$$\gamma(T) = 0.075\,478\,7 - 0.000\,138\,489T - 0.336\,392\times 10^{(-6)}T^2 + 0.475\,362\times 10^{(-9)}T^3 + 0.264\,479\times 10^{(-9)}T^4, \quad \text{(A2)}$$

the dynamic viscosity [64]

$$\eta(T) = 0.001\,792 - 6.267\,241\times 10^{(-5)}T + 1.567\,118\,5\times 10^{(-6)}T^2 - 5.306\,324\,2\times 10^{(-9)}T^3 - 1.764\,882\,744\times 10^{(-9)}T^4 - 2.799\,21\times 10^{(-10)}T^5, \quad \text{(A3)}$$

the thermal conductivity [66]

$$\kappa(T) = 0.560\,43 + 0.002\,074\,9T - 7.919\,24\times 10^{(-6)}T^2 - 1.043\,04\times 10^{(-8)}T^3, \quad \text{(A4)}$$

and the saturation-vapor pressure [6]

$$P_s = 611.2 \exp[1045.851\,157\,7 - 21\,394.666\,262\,9/(T + 273.12) + 1.096\,904\,4(T + 273.12) - 1.300\,374\,1 \times 10^{(-3)}(T + 273.12)^2 + 7.747\,298\,4 \times 10^{(-7)}(T + 273.12)^3 - 2.164\,900\,5 \times 10^{(-12)}(T + 273.12)^4 - 211.389\,655\,9 \ln(T + 273.12)]. \quad \text{(A5)}$$

We also use the following thermodynamic relations to determine κ_T and c_p [6]:

$$\kappa_T = -\frac{1}{\rho}\frac{\partial \rho}{\partial T}, \quad \text{(A6)}$$

$$c_p^L(T) = c_p^V(T) - \frac{d}{dT}\left(\frac{RT^2}{P_s}\frac{dP_s}{dT}\right). \quad \text{(A7)}$$

[1] G. Fang and C. A. Ward, Phys. Rev. E **59**, 417 (1999).
[2] G. Fang and C. A. Ward, Phys. Rev. E **59**, 441 (1999).
[3] C. A. Ward and D. Stanga, Phys. Rev. E **64**, 051509 (2001).
[4] V. K. Badam, V. Kumar, F. Durst, and K. Danov, Exp. Therm. Fluid Sci. **32**, 276 (2007).
[5] C. A. Ward and G. Fang, Phys. Rev. E **59**, 429 (1999).
[6] F. Duan, I. Thompson, and C. A. Ward, J. Phys. Chem. B **112**, 8605 (2008).
[7] R. Holyst and M. Litniewski, J. Chem. Phys. **130**, 074707 (2009).
[8] R. Holyst and M. Litniewski, Phys. Rev. Lett. **100**, 055701 (2008).
[9] R. Marek and J. Straub, Int. J. Heat Mass Transfer **44**, 39 (2001).
[10] R. B. Currie and L. F. Phillips, J. Non-Equilib. Thermodyn. **34**, 265 (2009).
[11] A. Onuki, Phys. Rev. E **79**, 046311 (2009).
[12] H. K. Dhavaleswarapu, S. V. Garimella, and J. Y. Murthy, ASME J. Heat Transfer **131**, 061501 (2009).
[13] S. Wan, J. Zhao, and G. Liu, J. Therm. Sci. **18**, 13 (2009).
[14] F. Duan, J. Phys. D **42**, 102004 (2009).
[15] D. Gazzola, E. F. Scarselli, and R. Guerrieri, Microfluid. Nanofluid. **7**, 659 (2009).
[16] C. A. Ward and F. Duan, Phys. Rev. E **69**, 056308 (2004).
[17] F. Duan and C. A. Ward, Phys. Rev. E **72**, 056302 (2005).
[18] F. Duan, V. K. Badam, F. Durst, and C. A. Ward, Phys. Rev. E **72**, 056303 (2005).
[19] F. Duan and C. A. Ward, Phys. Rev. E **72**, 056304 (2005).
[20] K. S. Das and C. A. Ward, Phys. Rev. E **75**, 065303(R) (2007).
[21] I. Thompson, F. Duan, and C. A. Ward, Phys. Rev. E **80**, 056308 (2009).
[22] J. R. A. Pearson, J. Fluid Mech. **4**, 489 (1958).
[23] D. A. Nield, J. Fluid Mech. **19**, 341 (1964).
[24] C. Panzarella and M. Kassemi, Int. J. Heat Mass Transfer **52**, 3767 (2009).
[25] H. J. Palmer and J. C. Berg, J. Fluid Mech. **47**, 779 (1971).
[26] E. L. Koschmieder and M. I. Biggerstaff, J. Fluid Mech. **167**, 49 (1986).
[27] M. F. Schatz, S. J. VanHook, W. D. McCormick, J. B. Swift, and H. L. Swinney, Phys. Rev. Lett. **75**, 1938 (1995).
[28] A.-T. Chai and N. Zhang, Experimental Heat Transfer **11**, 187 (1998).
[29] G. T. Barnes and A. I. Feher, J. Colloid Interface Sci. **75**, 584 (1980).
[30] G. T. Barnes and D. S. Hunter, J. Colloid Interface Sci. **88**, 437 (1982).
[31] H. K. Cammenga, D. Schreiber, and B.-E. Rudolph, J. Colloid Interface Sci. **92**, 181 (1983).
[32] H. K. Cammenga, D. Schreiber, G. T. Barnes, and D. S. Hunter, J. Colloid Interface Sci. **98**, 585 (1984).
[33] X. Xu and J. Luo, Appl. Phys. Lett. **91**, 124102 (2007).
[34] S. Rosenblat, G. M. Homsy, and S. H. Davis, J. Fluid Mech. **120**, 123 (1982).
[35] S. Rosenblat, H. G. M., and S. H. Davis, J. Fluid Mech. **120**, 91 (1982).
[36] P. C. Dauby, G. Lebon, P. Colinet, and J. C. Legros, Q. J. Mech. Appl. Math. **46**, 683 (1993).
[37] D. Krmpotić, G. B. Mindlin, and C. Perez-Garcia, Phys. Rev. E **54**, 3609 (1996).
[38] D. Schwabe, Exp. Fluids **40**, 942 (2006).
[39] R. Liu and Q. Liu, Acta Mech. Sin. **22**, 109 (2006).
[40] R. Liu and Q.-S. Liu, Chin. Phys. Lett. **23**, 879 (2006).
[41] R. Liu, Q.-S. Liu, and W.-R. Hu, Chin. Phys. Lett. **22**, 402 (2005).
[42] R. Liu and Q. Liu, Microgravity Sci. Technol. **21**, 233 (2009).
[43] J. Margerit, P. Colinet, G. Lebon, C. S. Iorio, and J. C. Legros, Phys. Rev. E **68**, 041601 (2003).
[44] A. Prosperetti and M. S. Plesset, Phys. Fluids **27**, 1590 (1984).
[45] M. Plesset, J. Chem. Phys. **20**, 790 (1952).
[46] M. S. Plesset and A. Prosperetti, J. Fluid Mech. **78**, 433 (1976).
[47] J. P. Burelbach, S. G. Bankoff, and S. H. Davis, J. Fluid Mech. **195**, 463 (1988).
[48] L. Y. Barash, T. P. Bigioni, V. M. Vinokur, and L. N. Shchur, Phys. Rev. E **79**, 046301 (2009).
[49] F. Girard, M. Antoni, S. Faure, and A. Steinchen, Langmuir **22**, 11085 (2006).
[50] F. Duan, C. A. Ward, V. K. Badam, and F. Durst, Phys. Rev. E **78**, 041130 (2008).
[51] P. Rahimi and C. A. Ward, Int. J. Thermodyn. **8**, 1 (2005).
[52] C. A. Ward, J. Non-Equilib. Thermodyn. **27**, 289 (2002).
[53] C. Ferrera, J. M. Montanero, A. Mialdun, V. M. Shevtsova, and M. G. Cabezas, Meas. Sci. Technol. **19**, 015410 (2007).
[54] S. Chandrasekhar, *Hydrodynamic and Hydromagnetic Stability*, 1st ed. (Oxford University Press, London, 1961), pp. 20–21.
[55] L. Landau and E. M. Lifschitz, *Fluid Mechanics*, 2nd ed. (Pergamon Press Ltd., London, 1987).
[56] A. Thess and S. A. Orszag, J. Fluid Mech. **283**, 201 (1995).
[57] J. S. Vrentas and C. M. Vrentas, Chem. Eng. Sci. **59**, 4433 (2004).
[58] A. Vidal and A. Acrivos, Phys. Fluids **9**, 615 (1966).
[59] P. G. Drazin, *Introduction to Hydrodynamic Stability* (Cambridge University Press, Cambridge, 2002), p. 97.

[60] D. Johnson and R. Narayanan, Phys. Rev. E **54**, R3102 (1996).
[61] S. Popov, A. Melling, F. Durst, and C. A. Ward, Int. J. Heat Mass Transfer **48**, 2299 (2005).
[62] K. Hisatake, S. Tanaka, and Y. Aizawa, J. Appl. Phys. **73**, 7395 (1993).
[63] A. J. H. McGaughey and C. A. Ward, J. Appl. Phys. **91**, 6406 (2002).
[64] *Handbook of Chemistry and Physics*, edited by R. C. Weast (Chemical Rubber Co., Cleveland, OH, 1971).
[65] K. Feldkamp, Chem.-Ing.-Tech. **41**, 1181 (1969).
[66] J. V. Sengers and J. T. R. Watson, J. Phys. Chem. Ref. Data **15**, 1291 (1986).